21 Yamashina A *et al.* Brachial–ankle pulse wave velocity as a marker of atherosclerotic vascular damage and cardiovascular risk. *Hypertens Res* 2003; **26**: 615–622.
22 Asmar R *et al.* Pulse pressure and aortic pulse wave are markers of cardiovascular risk in hypertensive populations. *Am J Hypertens* 2001; **14**: 91–97.
23 Guerin AP *et al.* Impact of aortic stiffness attenuation on survival of patients in end-stage renal failure. *Circulation* 2001; **103**: 987–992.
24 Peters MJ, Heyderman RS, Hatch DJ, Klein NJ. Investigation of platelet–neutrophil interactions in whole blood by flow cytometry. *J Immunol Methods* 1997; **209**: 125–135.
25 Hirai T, Sasayama S, Kawasaki T, Yagi S. Stiffness of systemic arteries in patients with myocardial infarction. A noninvasive method to predict severity of coronary atherosclerosis. *Circulation* 1989; **80**: 78–86.
26 Popele NM *et al.* Association between arterial stiffness and atherosclerosis: the Rotterdam Study. *Stroke* 2001; **32**: 454–460.
27 Blann AD, Lip GY, Beevers DG, McCollum CN. Soluble P-selectin in atherosclerosis: a comparison with endothelial cell and platelet markers. *Thromb Haemost* 1997; **77**: 1077–1080.
28 Bonfanti R, Furie BC, Furie B, Wagner DD. PADGEM (GMP140) is a component of Weibel–Palade bodies of human endothelial cells. *Blood* 1989; **73**: 1109–1112.
29 Hebert PR, Hennekens CH. An overview of the 4 randomized trials of aspirin therapy in the primary prevention of vascular disease. *Arch Intern Med* 2000; **160**: 3123–3127.
30 Goto S *et al.* Effects of ticlopidine on von Willebrand factor-mediated shear-induced platelet activation and aggregation. *Platelets* 2001; **12**: 406–414.
31 Nichols WW, O'Rourke MF. Effect of age and of hypertension on wave travel and reflections. *Arterial Vasodilation: Mechanisms and Therapy.* Arnold: London, 1993.
32 Kobayashi K *et al.* Interrelationship between noninvasive measurements of atherosclerosis: flow-mediated dilation of brachial artery, carotid intima-media thickness and pulse wave velocity. *Atherosclerosis* 2004; **173**: 13–18.
33 Dzau VJ, Gibbons GH. Vascular remodeling: mechanisms and implications. *J Cardiovasc Pharmacol* 1993; **21**: S1–S5.

Acetylcholine from vagal stimulation protects cardiomyocytes against ischemia and hypoxia involving additive non-hypoxic induction of HIF-1α

Yoshihiko Kakinuma[a,*], Motonori Ando[a], Masanori Kuwabara[b], Rajesh G. Katare[a], Koji Okudela[c], Masanobu Kobayashi[d], Takayuki Sato[a]

[a] *Department of Cardiovascular Control, Kochi Medical School, Nankoku 783-8505, Japan*
[b] *Department of Medicine and Geriatrics, Kochi Medical School, Nankoku, Japan*
[c] *Departmentof Pathology, Division of Cellular Pathobiology, Yokohama City University Graduate School of Medicine, Yokohama, Japan*
[d] *Division of Cancer Pathobiology, Institute for Genetic Medicine, Hokkaido University, Sapporo, Japan*

Received 20 December 2004; revised 2 February 2005; accepted 15 February 2005

Available online 13 March 2005

Edited by Angel Nebreda

Abstract Electrical stimulation of the vagal efferent nerve improves the survival of myocardial infarcted rats. However, the mechanism for this beneficial effect is unclear. We investigated the effect of acetylcholine (ACh) on hypoxia-inducible factor (HIF)-1α using rat cardiomyocytes under normoxia and hypoxia. ACh posttranslationally regulated HIF-1α and increased its protein level under normoxia. ACh increased Akt phosphorylation, and wortmannin or atropine blocked this effect. Hypoxia-induced caspase-3 activation and mitochondrial membrane potential collapse were prevented by ACh. Dominant-negative HIF-1α inhibited the cell protective effect of ACh. In acute myocardial ischemia, vagal nerve stimulation increased HIF-1α expression and reduced the infarct size. These results suggest that ACh and vagal stimulation protect cardiomyocytes through the PI3K/Akt/HIF-1α pathway.

Keywords: Acetylcholine; Ischemia; Apoptosis; Protein kinases

1. Introduction

The prognosis of patients with chronic heart failure remains poor, due to progressive remodeling of the heart and lethal arrhythmia. Acute ischemia or hypoxia causes loss of cardiomyocytes, followed by remodeling in the chronic phase. Although various therapeutic approaches have been introduced, including implantable defibrillators [1], a more effective modality of therapy has been anticipated for several years. A recent animal study by Li et al. [2] demonstrated that vagal nerve stimulation prevented ventricular remodeling after myocardial infarction, suggesting a novel therapeutic strategy against heart failure. Furthermore, Krieg et al. [3] reported that acetylcholine (ACh) has a cardioprotective effect. Although nitric oxide (NO) is supposed to be a major signaling molecule induced by ACh, a mechanism for the beneficial effect of vagal nerve stimulation on cardiomyocytes remains to be clarified. To investigate this mechanism, we hypothesized that vagal stimulation or ACh directly triggers a cell survival signal that is subsequently amplified and leads to protection of the cardiomyocytes from acute ischemic conditions, and that this effect of ACh, if continued, could be responsible for chronic cardioprotection.

In the present study, we focused on demonstrating the cellular action of ACh through hypoxia-inducible factor (HIF)-1α. HIF-1α is a transcription factor that is important for cell survival under hypoxia. HIF-1α activates the expression of many genes indispensable for cell survival [4,5]. Under normoxia, the HIF-1α protein level is very low, due to proteasomal degradation through with von Hippel–Lindau tumor suppressor protein (VHL). However, HIF-1α escapes from this degradation under hypoxia, and this is recognized as the hypoxic pathway [6,7]. Recently, it was revealed that HIF-1α can be also induced via a non-hypoxic pathway by angiotensin II [8,9]. Taken together, it is conceivable that HIF-1α induction is one of the adaptation processes to hypoxia and ischemia, and that additional induction of HIF-1α during ischemia via a non-hypoxic pathway could provide further cardioprotection.

Therefore, we investigated the direct effects of ACh on survival signaling in cardiomyocytes and of vagal stimulation on hearts. The results suggest that ACh and vagal stimulation protect cardiomyocytes from acute hypoxia and ischemia via additional HIF-1α protein induction through a non-hypoxic pathway.

2. Materials and methods

2.1. Cell culture

To examine the effect of ACh on cardiomyocytes, H9c2 cells as well as primary cardiomyocytes isolated from neonatal rats were used. H9c2 cells, which are frequently used to investigate signal transduction and channels in rat cardiomyocytes, are derived from rat embryonic ventricular cardiomyocytes. H9c2 cells were incubated in Dulbecco's modified Eagle's medium (DMEM) containing 10% fetal bovine serum (FBS) and antibiotics. Primary cardiomyocytes were isolated from 2–3-day-old neonatal WKY rats and incubated in DMEM/Ham F-12 containing 10% FBS. HEK293 cells and HeLa cells cultured in DMEM containing 10% FBS were also used.

2.2. Western Blot analysis

H9c2 cells and primary cardiomyocytes were treated with 1 mM ACh to evaluate expression of HIF-1α protein under normoxia or with 1 mM *S*-nitroso-*N*-acetylpenicillamine (SNAP) to study the signal transduction. To investigate the signal transduction, H9c2 cells were pretreated with a PI3K inhibitor, (wortmannin; 300 nM), a muscarinic receptor, (atropine; 1 mM), a transcriptional inhibitor, (actinomycin D; 0.5 μg/ml) or a protein synthesis inhibitor, (cycloheximide; 10 μg/ml), followed by ACh treatment. Cell lysates were mixed with a sample

*Corresponding author. Fax: +81 88 880 2310.
E-mail address: kakinuma@med.kochi-u.ac.jp (Y. Kakinuma).

0014-5793/$30.00
doi:10.1016/j.febslet.2005.02.065

buffer, fractionated by 10% SDS–PAGE and transferred onto membranes. The membranes were incubated with primary antibodies against HIF-1α (Santa Cruz Biotechnology, Santa Cruz, CA, USA), Akt and phospho-Akt (Cell Signaling Technology, Beverly, MA, USA), and α-tubulin (Lab Vision, Fremont, CA, USA), and then reacted with an HRP-conjugated secondary antibody (BD Transduction Laboratories, San Diego, CA, USA). Positive signals were detected with an enhanced chemiluminescence system (Amersham, Piscataway, NJ, USA). In each study, the experiments were performed in duplicate and repeated 3–5 times ($n = 3$–5). Representative data are shown.

2.3. MTT activity assay

To evaluate the effects of hypoxia and ACh on the mitochondrial function of cardiomyocytes, we measured 3-(4,5-dimethylthiazol-2-yl)-2,5-diphenyl tetrazolium bromide (MTT) reduction activity in H9c2 or HEK293 cells under hypoxia (1% oxygen concentration), in the presence or absence of ACh. The cells were pretreated with 1 mM ACh for 12 h, and then subjected to hypoxia for 12 h. At 4 h before sampling, the MTT reagents were added to the culture and incubated.

2.4. Caspase-3 activity assay

Caspase-3 activity was measured using a CPP32/Caspase-3 Fluorometric Protease Assay Kit, (Chemicon International, Temecula, CA, USA). Hypoxia-treated H9c2 cells with or without 1 mM ACh pretreatment were lysed and the cytosolic extract was added to the caspase-3 substrate. A fluorometer equipped with a 400-nm excitation filter and 505-nm emission filter was used to measure the samples.

2.5. DePsipher assay

To examine the effects of hypoxia and ACh on the mitochondrial electrochemical gradient, we analyzed cardiomyocytes using a DePsipher™ Mitochondrial Potential Assay Kit (Trevigen, Gaithersburg, Maryland, USA). Apoptotic cells, which undergo mitochondrial membrane potential collapse cannot accumulate the DePsipher reagent in their mitochondria. As a result, apoptotic cells show decreased red fluorescence in their mitochondria, and the reagent remains in the cytoplasm as a green fluorescent monomer. Therefore, apoptotic cells were easily differentiated from healthy cells, which showed more red fluorescence.

2.6. Evaluation of NO production

NO production was measured using the 4,5-diaminofluoresceindiacetate (DAF-2DA; Alexis, Lausen, Switzerland) fluorometric NO detection system as previously reported [10]. The intensity of the DAF-2DA green fluorescence in ACh-treated cells was measured and compared with that in non-treated cells (λ_{Ex} 492 nm; λ_{Em} 515 nm).

2.7. Transfection

To investigate the direct contribution of Akt phosphorylation to HIF-1α stabilization or that of HIF-1α to the ACh effect, HEK293 cells were transfected with an expression vector for wild-type Akt (wt Akt), dominant-negative Akt (dn Akt) [11], wild-type HIF-1α (wt HIF-1α) [12] or dominant-negative HIF-1α (dn HIF-1α), using Effectene (Qiagen, Valencia, CA, USA) according to the manufacture's protocol. After transfection, HEK293 cells were pretreated with 1 mM ACh for 12 h, followed by evaluating the HIF-1α protein level or by hypoxia for 12 h and MTT activity in each group was evaluated. As a control, cells were transfected with a vector for green fluorescent protein (GFP).

2.8. RT-PCR

Total RNA was isolated from H9c2 cells according to a modified acid guanidinium–phenol–chloroform method using an RNA isolation kit (ISOGEN; Nippon Gene, Tokyo, Japan), and reverse-transcribed to obtain a first-strand cDNA. This first-strand cDNA was amplified by specific primers for HIF-1α, and the PCR products were fractionated by electrophoresis.

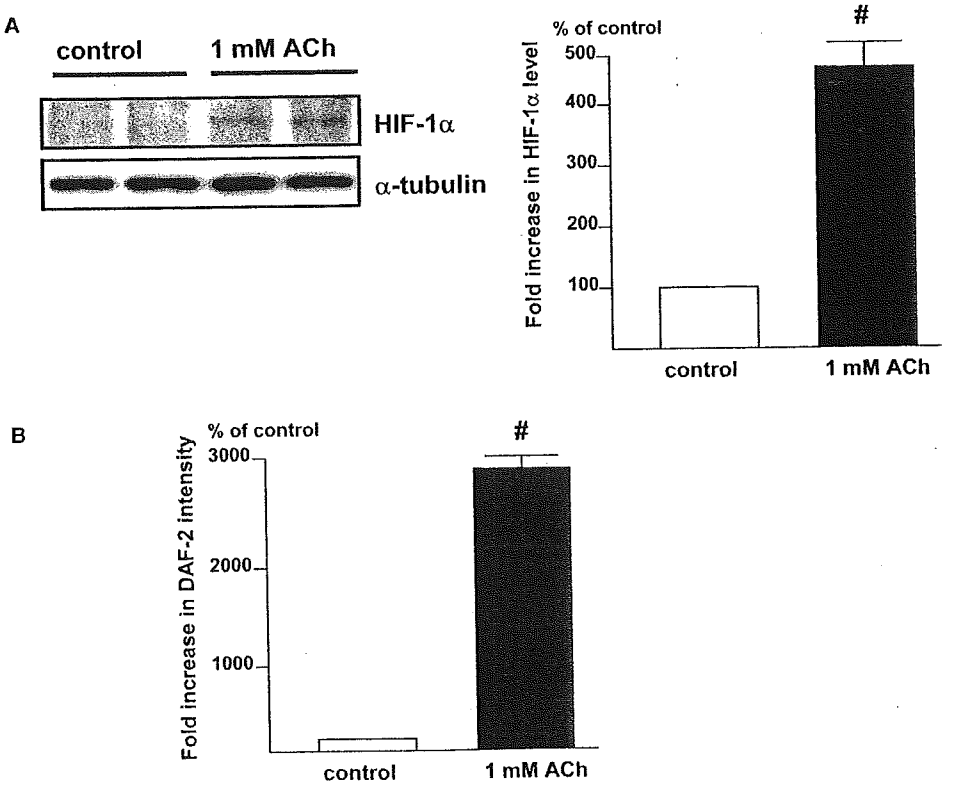

Fig. 1. HIF-1α is induced by ACh in rat cardiomyocytes even under normoxia. (A) After treatment of H9c2 cells with 1 mM ACh for 8 h, the HIF-1α protein level is increased ($^{\#}P < 0.05$ vs. control, $n = 4$). (B) ACh (1 mM) increases the intensity of DAF-2DA fluorescence ($^{\#}P < 0.01$ vs. control, $n = 3$).

2.9. Vagal nerve stimulation in myocardial ischemia

Left ventricular myocardial ischemia (MI) was performed by 3 h of left coronary artery (LCA) ligation in anesthetized 9-week-old male Wistar rats under artificial ventilation previously described [2]. Sham-operated (control) rats did not undergo LCA ligation. For vagal nerve stimulation (VS), the right vagal nerve in the neck was isolated and cut. Only the distal end of the vagal nerve was stimulated in order to exclude the effects of the vagal afferent. The electrode was connected to an isolated constant voltage stimulator. VS was performed from 1 min before the LCA ligation until 3 h afterwards, using 0.1 ms pulses at 10 Hz (MI-VS). The electrical voltage of the pulses was adjusted to obtain a 10% reduction in the heart rate before LCA ligation, but VS (MI-VS) was not associated with any blood pressure reduction during the experiments, compared with MI. At the end of the experiments, the rats were either injected with 2 ml of 2% Evans blue dye via the femoral vein to measure the risk area followed by determination of the infarct size with 2% triphenyl tetrazolium chloride (TTC) staining or the heart was excised for protein isolation and subsequent Western Blotting to detect HIF-1α protein. The percentage of the infarcted area of the left ventricle was calculated as the ratio of the infarcted area to the risk area.

2.10. Densitometry

The Western Blotting data were analyzed using Kodak 1D Image Analysis Software (Eastman Kodak Co., Rochester, NY, USA).

2.11. Statistics

The data were presented as means ± S.E. The mean values between two groups were compared by the unpaired Student's *t* test. Differences among data were assessed by ANOVA for multiple comparisons of results. Differences were considered significant at $P < 0.05$.

3. Results

3.1. Posttranslational regulation of HIF-1α by ACh through a non-hypoxic pathway

ACh (1 mM) increased HIF-1α protein expression in H9c2 cells under normoxia (Fig. 1A). ACh increased NO production, as evaluated by DAF-2DA (Fig. 1B), suggesting that

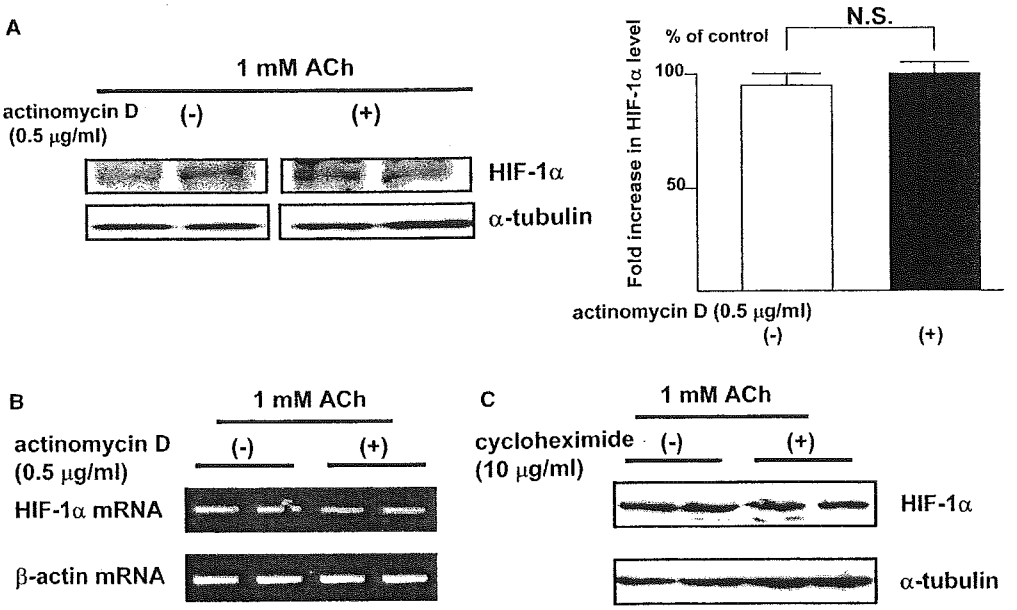

Fig. 2. HIF-1α induction by ACh is posttranslationally regulated in rat cardiomyocytes under normoxia. (A) The HIF-1α protein level in H9c2 cells in the presence of 0.5 μg/ml of actinomycin D is increased by 1 mM ACh to a comparable level to that in the absence of actinomycin D (N.S., not significant, $n = 3$). (B) Actinomycin D does not decrease the HIF-1α mRNA level, as evaluated by RT-PCR. (C) Cycloheximide (10 μg/ml) does not affect the HIF-1α protein level ($n = 3$).

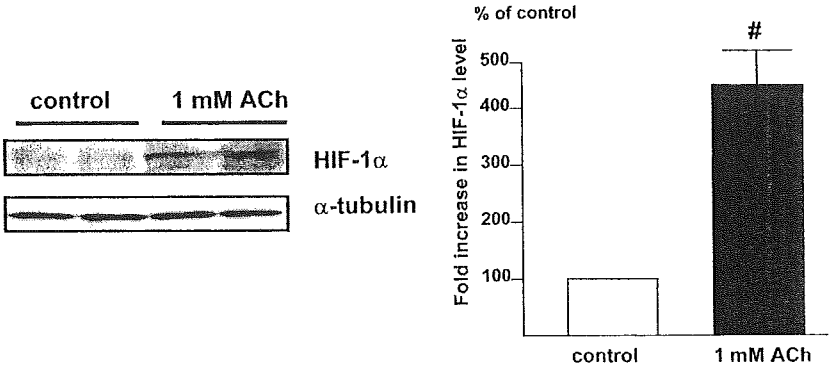

Fig. 3. Rat primary cultured cardiomyocytes show comparable HIF-1α induction by 1 mM ACh to that in H9c2 cells ($^{\#}P < 0.05$ vs. control, $n = 3$).

NO is involved in the signal transduction of HIF-1α induction. Actinomycin D (0.5 μg/ml; Figs. 2A and B) and cycloheximide (10 μg/ml; Fig. 2C) did not decrease the HIF-1α level under normoxia, suggesting that HIF-1α degradation is regulated by ACh. Furthermore, ACh increased HIF-1 α level in primary cardiomyocytes without reducing their beating rate (Fig. 3). Since H9c2 cells did not beat, these results suggest that HIF-1 induction is independent of the heart rate-decreasing effect of ACh.

3.2. Akt phosphorylation by ACh

ACh had no effect on the total Akt protein level, but increased Akt phosphorylation (Fig. 4A) as effectively as SNAP (data not shown). The ACh-induced Akt phosphorylation was inhibited by atropine in a dose-dependent manner (Fig. 4B). ACh-induced Akt phosphorylation and its inhibition by atropine were also observed in rat primary cardiomyocytes (Fig. 4C).

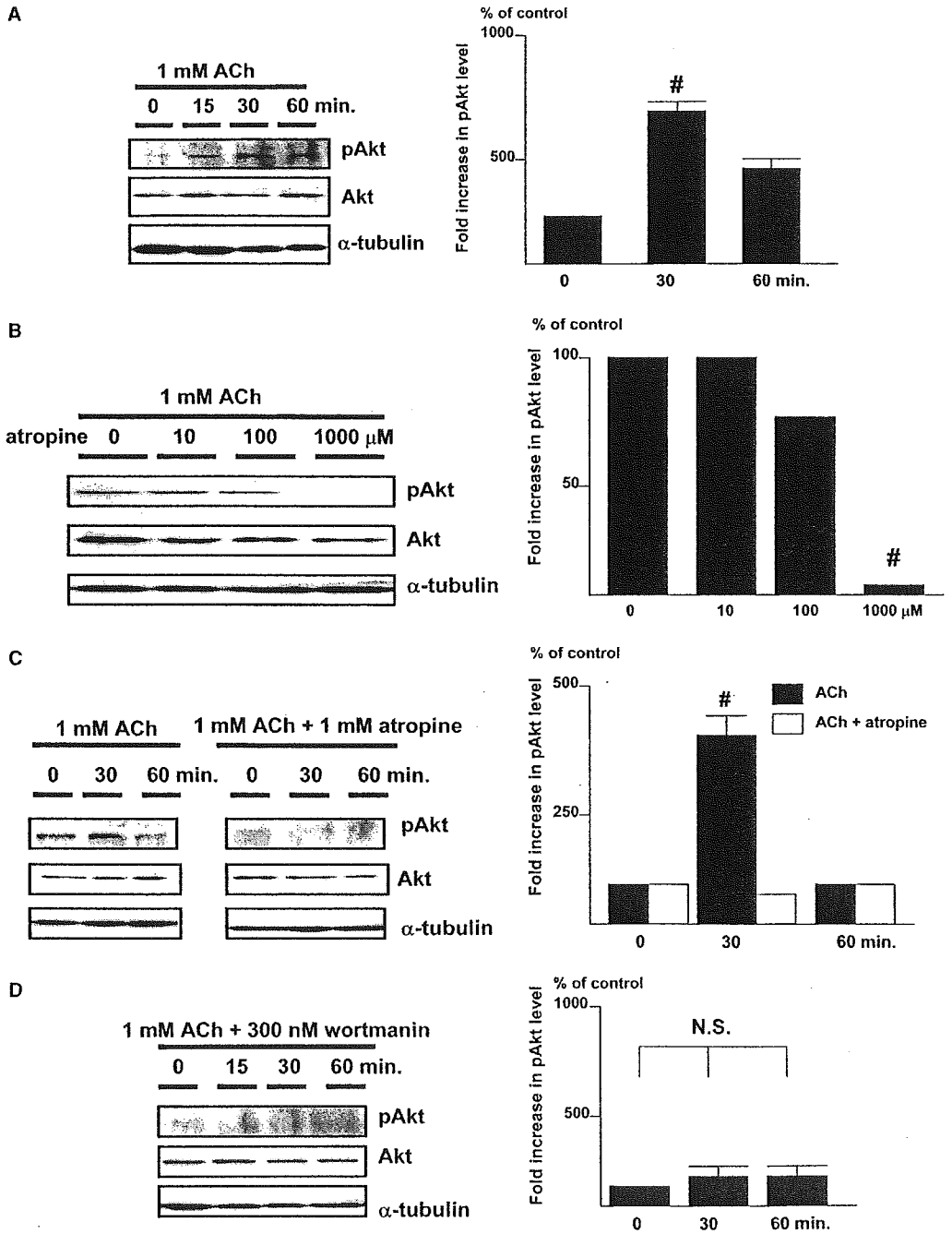

Fig. 4. Akt is activated by ACh in rat cardiomyocytes, leading to HIF-1α induction. (A) Akt phosphorylation in H9c2 cells is rapidly increased by 1 mM ACh ($^{\#}P < 0.05$ vs. baseline, $n = 4$), whereas the total protein level of Akt remains unaffected. (B) The ACh-induced increase in Akt phosphorylation is blocked by 1 mM atropine ($^{\#}P < 0.05$ vs. 0 μM atropine, $n = 3$). (C) ACh (1 mM) also increases Akt phosphorylation in rat primary cardiomyocytes ($^{\#}P < 0.05$ vs. baseline, $n = 3$), and atropine blocks this effect. (D) Pretreatment with 300 nM wortmannin completely inhibits ACh-induced Akt phosphorylation in H9c2 cells (N.S., not significant, $n = 3$). (E) Wortmannin (300 nM) also inhibits HIF-1α induction by ACh ($^{\#}P < 0.05$ vs. wortmannin (+), $n = 3$). Each figure shows a representative result from three independently performed experiments ($n = 3$). (F) In contrast to wt Akt, HIF-1α induction by ACh is blocked by dn Akt in HEK293 cells ($n = 4$).

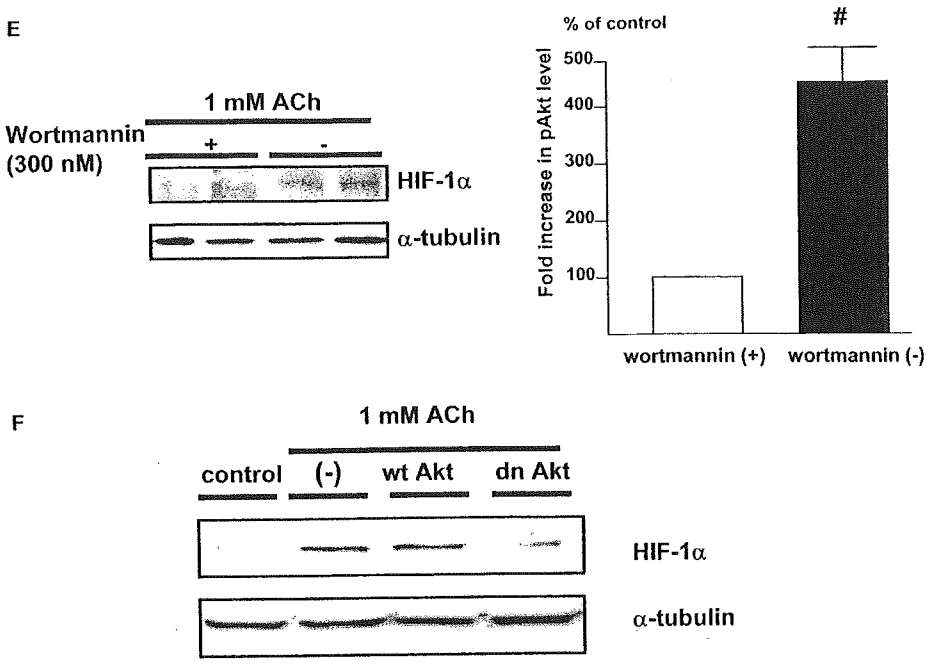

Fig. 4 (*continued*)

3.3. PI3K/Akt Pathway for HIF-1α induction by ACh

Wortmannin completely inhibited the ACh-induced Akt phosphorylation (Fig. 4D), in clear contrast to the data in Fig. 4A. Furthermore, it also attenuated the HIF-1α induction by ACh (Fig. 4E). To elucidate the contribution of Akt phosphorylation to HIF-1α protein level in normoxia, dn Akt was introduced into HEK293 cells, and found to partially inhibit the HIF-1α induction by ACh (Fig. 4F).

3.4. Effect of ACh on apoptosis during hypoxia

The DePsipher assay clearly showed that hypoxia (1% oxygen concentration) for 12 h caused mitochondrial membrane potential collapse leading to cell death, and that 1 mM ACh inhibited this collapse in H9c2 cells (Fig. 5A). ACh attenuated the decrease in MTT activity caused by 12 h of hypoxia in H9c2 cells (Fig. 5B; 103.4 ± 0.8% in ACh + hypoxia vs. 56.6 ± 0.7% in hypoxia, $P < 0.01$, $n = 8$) and HEK293 cells ($P < 0.01$ vs. hypoxia). The caspase-3 activity was increased by hypoxia in H9c2 cells, and pretreatment with 1 mM ACh inhibited this increase (Fig. 5C; 128 ± 2% in hypoxia vs. 90 ± 2% in ACh + hypoxia, $P < 0.01$, $n = 4$). To elucidate the dependency of the ACh-induced protective effect on HIF-1α, dn HIF-1α was transfected into HEK293 cells, followed by ACh pretreatment and then hypoxia. It was found that dn HIF-1α inhibited the protective effect of ACh from hypoxia (Fig. 5D; 115.1 ± 1.2% in wt HIF-1α and 111.8 ± 1.8% in GFP vs. 59.0 ± 3.4% in dn HIF-1α, $P < 0.05$, $n = 10$), suggesting that HIF-1α induction by ACh is partially responsible for the protective effect.

3.5. Effect of vagal stimulation on HIF-1α in myocardial ischemia

To evaluate the significance of ACh for cardioprotection in vivo, the vagal nerve was stimulated prior to the MI. Histological analysis demonstrated a tendency for the infarcted area from the vagal nerve-stimulated (MI-VS) hearts to be smaller than that from non-stimulated (MI) hearts (31.5 ± 4.6% in MI-VS vs. 40.9 ± 2.5% in MI, $n = 3$), even though the risk areas (non-perfused areas) were comparable (Fig. 6A; 59.2 ± 1.0% in MI-VS vs. 53.7 ± 1.0% in MI, $n = 3$). In the MI-VS hearts, the HIF-1α protein level was further elevated compared to that in the MI hearts (Fig. 6B; 244 ± 24% in MI-VS vs. 112 ± 1% in MI, $n = 3$). These results suggest that vagal nerve stimulation in the ischemic heart activates both the hypoxic and non-hypoxic pathways of HIF-1α induction, resulting in increased induction of HIF-1α.

3.6. Non-hypoxic induction of HIF-1α in other cells

The observed ACh-mediated HIF-1 induction was not limited to H9c2 or primary cultured cardiomyocytes, but also found in several other types of cell lines, including HEK293, and HeLa cells (Fig. 7). Since these cells did not beat spontaneously, the results suggest that the system of ACh-mediated HIF-1α induction is not only independent of the beating rate of cardiomyocytes, but also a generally conserved system in cells.

4. Discussion

4.1. Cardioprotective action by ACh and vagal stimulation via the muscarinic receptor

Using animal models, several studies have shown that accentuated antagonism against the sympathetic nervous system is a major mechanism for the beneficial effect of vagal tone on the ischemic heart [13]. Although ACh was involved in triggering preconditioning mechanisms in an ischemia-reperfusion model [3], it remained unclear whether vagal nerve stimulation in acute ischemia or hypoxia followed these mechanisms. In the present study, we have disclosed that ACh possesses a

protective effect on cardiomyocytes. In rat cardiomyocytes, ACh triggered a sequence of survival signals through Akt that eventually induced HIF-1α, inhibited the collapse of the mitochondrial membrane potential and decreased caspase-3 activity, thereby leading to the survival of cardiomyocytes under hypoxia. Furthermore, our results suggest ACh exerts this action through Akt in other cells. The current study therefore provides another insight into the cellular mechanism for the cardioprotective effects of ACh and vagal stimulation.

4.2. Signaling pathway of ACh via PI3K/Akt and antiapoptotic effects of ACh

Since previous studies demonstrated that a PI3K inhibitor greatly reduced HIF-1α induction in heart and renal cells [14,15] and a few studies have reported that MAP kinase is activated through ACh, we focused on the PI3K/Akt pathway, one of the important cell survival signaling pathways [16], and found that ACh directly activated Akt phosphorylation via PI3K. PI3K/Akt signaling has been reported to have an

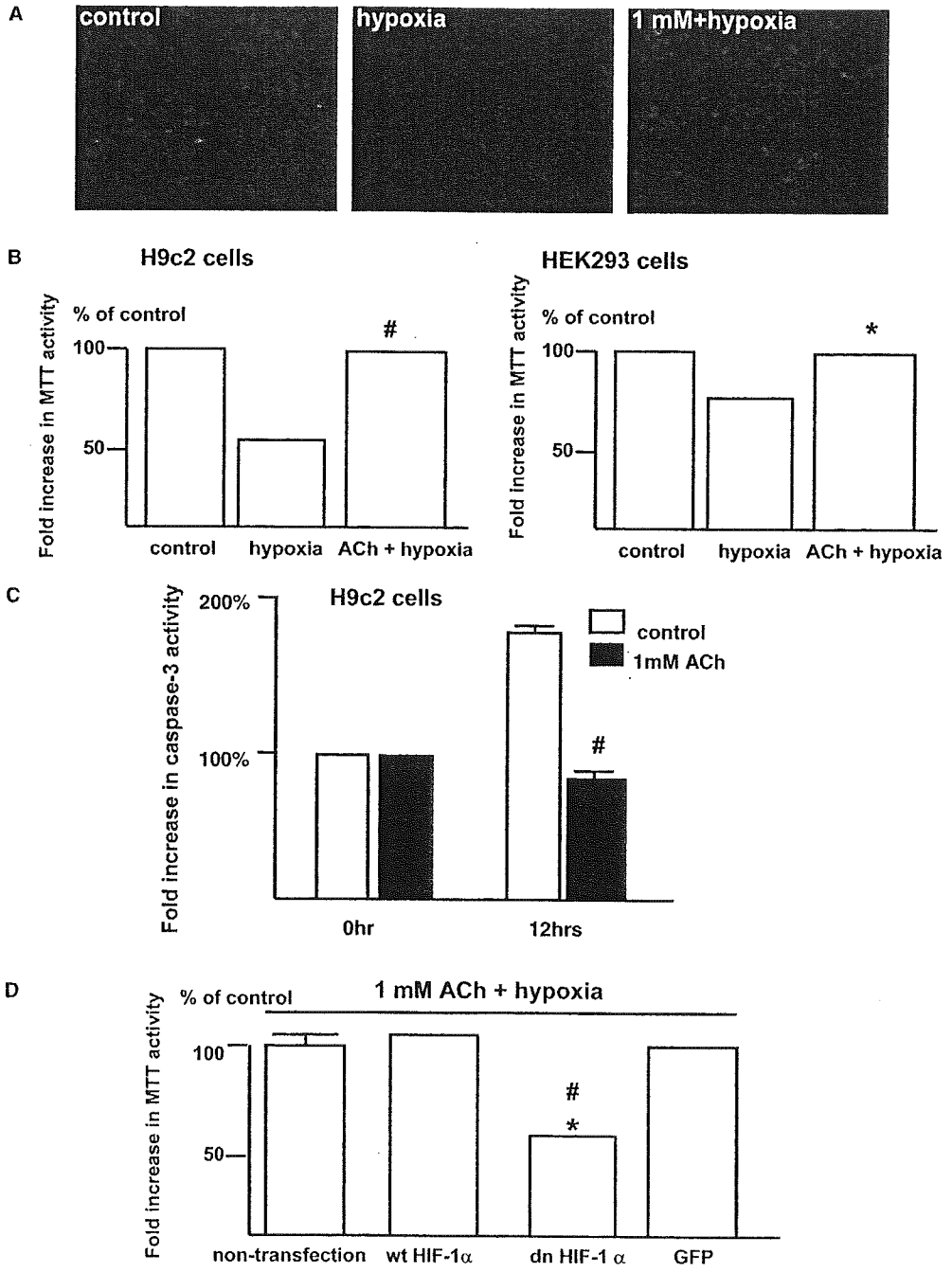

Fig. 5. Collapse of the mitochondrial membrane potential in rat cardiomyocytes under hypoxia is attenuated by ACh pretreatment. (A) Hypoxia decreases the mitochondrial membrane potential in H9c2 cells within 12 h. Red spots are decreased by hypoxia, whereas pretreatment with 1 mM ACh for 12 h inhibits this effect. (B) Pretreatment with 1 mM ACh inhibits the decrease in MTT reduction activity induced by 12 h of hypoxia not only in H9c2 cells ($^{\#}P < 0.01$ vs. hypoxia, $n = 8$) but also in HEK293 cells ($^{*}P < 0.01$ vs. hypoxia, $n = 8$). (C) Hypoxia increases caspase-3 activity, whereas pretreatment with 1 mM ACh inhibits this effect ($^{\#}P < 0.01$ vs. hypoxia, $n = 3$). (D) In contrast to wt HIF-1α or GFP, dn HIF-1α alone decreases the MTT activity under hypoxia after ACh treatment ($^{\#}P < 0.01$ vs. wt and GFP, $^{*}P < 0.05$ vs. non-transfection, $n = 10$).

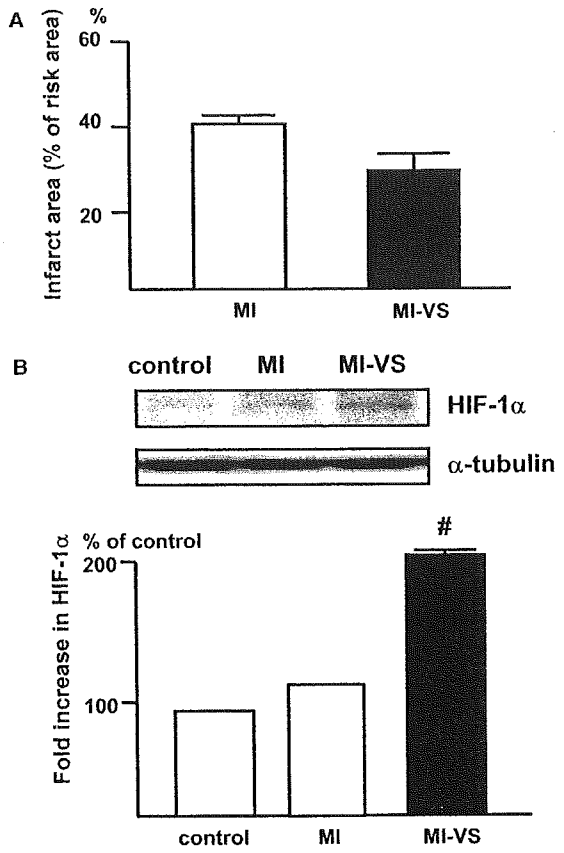

Fig. 6. Vagal nerve stimulation decreases infarcted area with increased HIF-1α expression. (A) A quantitative analysis reveals comparable non-perfused areas in both vagal-stimulated (MI-VS) and non-stimulated (MI) hearts, whereas the infarcted area identified by TTC staining is smaller in the MI-VS heart than in the MI heart. (B) HIF-1α induction in the ischemic heart is increased by vagal stimulation (MI-VS) compared with that in ischemia alone (MI) ($^{\#}P < 0.01$ vs. MI) ($n = 3$).

antiapoptotic activity through various features, such as inhibition of Bad-binding to Bcl-2, caspase 9, Fas and glycogen synthetase kinase-3 [17,18]. These facts imply a definite involvement of Akt activation in cell survival. As shown using dn HIF-1α, ACh inhibited hypoxia-induced cell death through HIF-1α induction via Akt phosphorylation. These results indicate that ACh actually protects cardiomyocytes from hypoxia at the cellular level.

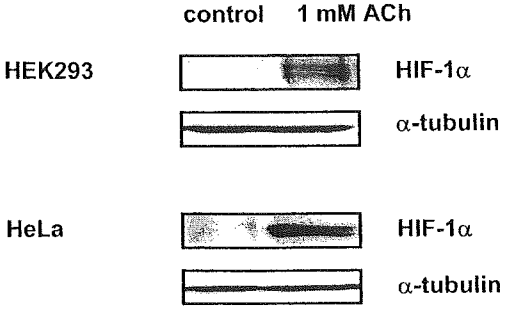

Fig. 7. HIF-1α is induced by ACh under normoxia in other cells. ACh (1 mM) increases HIF-1α protein level in HEK293 and HeLa cells ($n = 3$ each) under normoxia.

4.3. Additional induction of HIF-1α by ACh and vagal stimulation

HIF-1α regulates the transcriptional activities of very diverse genes involved in cell survival and is itself regulated at the posttranslational level by VHL [4,6,7]. Recent studies have shown that HIF-1α is also regulated through a non-hypoxic pathway involving angiotensin II, TNF-α and NO [8,9,19,20]. Therefore, it is speculated that cardiomyocytes possess a similar system for regulating HIF-1α through ACh, independent of the oxygen concentration. Induction of HIF-1α is a powerful cellular response against hypoxia, and further increases in its expression by other pathways may be beneficial. The present results indicate that the significance of ACh or vagal nerve stimulation in hypoxic stress can be attributed to additional HIF-1α induction through dual induction pathways, i.e., hypoxic and non-hypoxic pathways.

The present study has revealed that ACh-mediated HIF-1α induction is widely conserved in other cells. Consistent with a previous report [10], the current results suggest that NO is produced by ACh. According to a report that NO attenuates the interaction between pVHL and HIF-1α through inhibiting PHD activity [21], it is possible that ACh may increase the HIF-1α protein level through NO. Recent studies conducted by Krieg et al. [3] and Xi et al. [22], have provided supportive data compatible with our results, while another study by Hirota et al. [23] also revealed a non-hypoxic pathway for HIF-1α induction by ACh in a human kidney-derived cell line.

The signaling pathway of the muscarinic receptor has been studied extensively, and many pathways are involved in its specific biological effects. Therefore, possible involvement of other pathways in the non-hypoxic induction of HIF-1α cannot be excluded. However, it was demonstrated that dn Akt and dn HIF-1α decreased the effect of ACh. Consistent with a recent study [24], we have revealed that ACh or vagal stimulation protects cardiomyocytes in the acute phase. This observation suggests that the protective effect in the acute phase may result in inhibition of cardiac remodeling in the chronic phase, since vagal stimulation produces additional HIF-1α induction through a non-hypoxic pathway, which increases cell survival.

Acknowledgment: This study was supported by a Health and Labor Sciences Research Grant (H15-PHYSI-001) for Advanced Medical Technology from the Ministry of Health, Labor, and Welfare of Japan.

References

[1] Julian, D.G., Camm, A.J., Frangin, G., Janse, M.J., Munoz, A., Schwartz, P.J. and Simon, P. (1997) Randomised trial of effect of amiodarone on mortality in patients with left-ventricular dysfunction after recent myocardial infarction: EMIAT. European Myocardial Infarct Amiodarone Trial Investigators. Lancet 349, 667–674.

[2] Li, M., Zheng, C., Sato, T., Kawada, T., Sugimachi, M. and Sunagawa, K. (2004) Vagal nerve stimulation markedly improves long-term survival after chronic heart failure in rats. Circulation 109, 120–124.

[3] Krieg, T., Qin, Q., Philipp, S., Alexeyev, M.F., Cohen, M.V. and Downey, J.M. (2004) Acetylcholine and bradykinin trigger preconditioning in the heart through pathway that includes Akt and NOS. Am. J. Physiol. Heart Circ. Physiol. 287, H2606–H2611.

[4] Semenza, G.L. (2003) HIF-1, O(2), and the 3 PHDs: how animal cells signal hypoxia to the nucleus. Cell 107, 1–3.
[5] Kakinuma, Y., Miyauchi, T., Yuki, K., Murakoshi, N., Goto, K. and Yamaguchi, I. (2001) Novel molecular mechanism of increased myocardial endothelin-1 expression in the failing heart involving the transcriptional factor hypoxia-inducible factor-1α induced for impaired myocardial energy metabolism. Circulation 103, 2387–2394.
[6] Maxwell, P.H., Wiesener, M.S., Chang, G.W., Clifford, S.C., Vaux, E.C., Cockman, M.E., Wykoff, C.C., Pugh, C.W., Maher, E.R. and Ratcliffe, P.J. (1999) The tumour suppressor protein VHL targets hypoxia-inducible factors for oxygen-dependent proteolysis. Nature 399, 271–275.
[7] Min, J.H., Yang, H., Ivan, M., Gertler, F., Kaelin Jr, W.G. and Pavletich, N.P. (2002) Structure of an HIF-1alpha-pVHL complex: hydroxyproline recognition in signaling. Science 296, 1886–1889.
[8] Page, E.L., Robitaille, G.A., Pouyssegur, J. and Richard, D.E. (2002) Induction of hypoxia-inducible factor-1alpha by transcriptional and translational mechanisms. J. Biol. Chem. 277, 48403–48409.
[9] Richard, D.E., Berra, E. and Pouyssegur, J. (2000) Non-hypoxic pathway mediates the induction of hypoxia-inducible factor 1alpha in vascular smooth muscle cells. J. Biol. Chem. 275, 26765–26771.
[10] Zanella, B., Calonghi, N., Pagnotta, E., Masotti, L. and Guarnieri, C. (2002) Mitochondrial nitric oxide localization in H9c2 cells revealed by confocal microscopy. Biochem. Biophys. Res. Commun. 290, 1010–1014.
[11] Okudela, K., Hayashi, H., Ito, T., Yazawa, T., Suzuki, T., Nakane, Y., Sato, H., Ishi, H., KeQin, X., Masuda, A., Takahashi, T. and Kitamura, H. (2004) K-ras gene mutation enhances motility of immortalized airway cells and lung adenocarcinoma cells via Akt activation: possible contribution to non-invasive expansion of lung adenocarcinoma. Am. J. Pathol. 164, 91–100.
[12] Chen, J., Zhao, S., Nakada, K., Kuge, Y., Tamaki, N., Okada, F., Wang, J., Shindo, M., Higashino, F., Takeda, K., Asaka, M., Katoh, H., Sugiyama, T., Hosokawa, M. and Kobayashi, M. (2004) Dominant-negative hypoxia-inducible factor-1 alpha reduces tumorigenicity of pancreatic cancer cells through the suppression of glucose metabolism. Am. J. Pathol. 162, 1283–1291.
[13] Du, X.J., Dart, A.M., Riemersma, R.A. and Oliver, M.F. (1990) Failure of the cholinergic modulation of norepinephrine release during acute myocardial ischemia in the rat. Circ. Res. 66, 950–956.
[14] Kim, C.H., Cho, Y.S., Chun, Y.S., Park, J.W. and Kim, M.S. (2002) Early expression of myocardial HIF-1alpha in response to mechanical stresses: regulation by stretch-activated channels and the phosphatidylinositol 3-kinase signaling pathway. Circ. Res. 90, e25–e33.
[15] Sandau, K.B., Zhou, J., Kietzmann, T. and Brune, B. (2001) Regulation of the hypoxia-inducible factor 1alpha by the inflammatory mediators nitric oxide and tumor necrosis factor-alpha in contrast to desferroxamine and phenylarsine oxide. J. Biol. Chem. 276, 39805–39811.
[16] Vanhaesebroeck, B. and Alessi, D.R. (1999) The regulation and activities of the multifunctional serine/threonine kinase Akt/PKB. Exp. Cell Res. 253, 210–229.
[17] Kennedy, S.G., Wagner, A.J., Conzen, S.D., Jordan, J., Bellacosa, A., Tsichlis, P.N. and Hay, N. (1997) The PI3-kinase/Akt signaling pathway delivers an anti-apoptotic signal. Genes Dev. 11, 701–713.
[18] Cross, D.A., Alessi, D.R., Cohen, P., Andjelkovich, M., Hemmings, B.A. and Inhibition of glycogen synthase kinase-3 by insulin mediated by protein kinase, B. (1995) Nature 378, 785–789.
[19] Zhou, J., Schmid, T. and Brune, B. (2003) Tumor necrosis factor-alpha causes accumulation of a ubiquitinated form of hypoxia inducible factor-1alpha through a nuclear factor-kappaB-dependent pathway. Mol. Biol. Cell 14, 2216–2225.
[20] Sandau, K.B., Fandrey, J. and Brune, B. (2001) Accumulation of HIF-1alpha under the influence of nitric oxide. Blood 97, 1009–1015.
[21] Metzen, E., Zhou, J., Jelkmann, W., Fandrey, J. and Brune, B. (2003) Nitric oxide impairs normoxic degradation of HIF-1alpha by inhibition of prolyl hydroxylases. Mol. Biol. Cell 14, 3470–3481.
[22] Xi, L., Taher, M., Yin, C., Salloum, F. and Kukreja, R.C. (2004) Cobalt chloride induces delayed cardiac preconditioning in mice through selective activation of HIF-1{alpha}/AP-1 and iNOS signaling. Am. J. Physiol. Heart. Circ. Physiol. 287, H2369–H2375.
[23] Hirota, K., Fukuda, R., Takabuchi, S., Kizaka-Kondoh, S., Adachi, T., Fukuda, K. and Semenza, G.L. (2004) Induction of hypoxia-inducible factor 1 activity by muscarinic acetylcholine receptor signaling. J. Biol. Chem. 279, 41521–41528.
[24] Wang, H., Yu, M., Ochani, M., Amella, C.A., Tanovic, M., Susarla, S., Li, J.H., Wang, H., Yang, H., Ulloa, L., Al-Abed, Y., Czura, C.J. and Tracey, K.J. (2003) Nicotinic acetylcholine receptor alpha7 subunit is an essential regulator of inflammation. Nature 421, 384–388.

Effect of Serum Albumin on QRS Wave Amplitude in Patients Free of Heart Disease

Yoshihiro Kudo, MD, Fumiyasu Yamasaki, MD, Hiromi Kataoka, MS, Yoshinori Doi, MD, and Tetsuro Sugiura, MD

We studied 193 patients free of heart disease to determine the relation between QRS amplitude and serum albumin. Although there were no significant differences in echocardiographic indexes between the 2 groups, albumin (35.1 ± 4.3 vs 40.1 ± 3.2 g/L) and colloid osmotic pressure (21 ± 4 vs 24 ± 3 mm Hg) were significantly lower in patients with low voltages compared with those without. Moreover, there was a good relation (r = 0.78) between change in QRS amplitude and change in albumin concentration. ©2005 by Excerpta Medica Inc.
(Am J Cardiol 2005;95:789–791)

Low voltage is 1 of the electrocardiographic manifestations in patients with pericardial effusion,[1–4] but it is also found in other disorders, including myocardial disease, lung disease, hypothyroidism, and obesity. [5] Serum albumin has been reported to have a direct correlation with QRS amplitude[6]; other investigators found an inverse relation between QRS amplitude and body weight in patients with anasarca.[7] However, as anasarca is frequently associated with decreased albumin concentration, the particular effect of albumin in modulating electrocardiographic voltage is yet to be defined. Accordingly, we designed a study to determine the effect of albumin concentration on QRS wave amplitude in patients free of heart and lung diseases.

• • •

Among 5,766 consecutive patients who were referred to our echocardiography laboratory between January 1, 1998, and December 31, 2001, we investigated 193 clinically stable patients (aged 41 to 95 years) with no history of heart or lung disease and no electrocardiographic, chest radiographic, or echocar-

From the Departments of Laboratory Medicine and Medicine and Geriatrics, Kochi Medical School, Kochi, Japan. Dr. Sugiura's address is: Department of Laboratory Medicine, Kochi Medical School, Kohasu Oko-cho Nankoku City, Kochi 783-8505, Japan. E-mail: sugiurat@med.kochi-u.ac.jp. Manuscript received August 30, 2004; revised manuscript received and accepted November 18, 2004.

0002-9149/05/$–see front matter
doi:10.1016/j.amjcard.2004.11.040

TABLE 1 Baseline Characteristics

Variable	Low Voltage: Present (n = 35)	Low Voltage: Absent (n = 158)	p Value
Age (yrs)	70 ± 12	67 ± 10	0.124
Men/women	14/21	69/89	0.835
Body mass index (kg/m^2)	21.5 ± 3.2	22.3 ± 4.1	0.280
Albumin (g/L)	35.1 ± 4.3	40.1 ± 3.2	<0.001
Globulin (g/L)	26.3 ± 6.6	27.1 ± 5.8	0.473
Total protein (g/L)	61.5 ± 8.7	67.2 ± 6.4	<0.001
Colloid osmotic pressure (mm Hg)	21 ± 4	24 ± 3	<0.001
Hematocrit (%)	36.2 ± 4.3	37.7 ± 4.6	0.078

TABLE 2 Echocardiographic Indexes

Variable	Low Voltage: Present (n = 35)	Low Voltage: Absent (n = 158)	p Value
Left ventricular			
Ejection fraction (%)	70 ± 7	70 ± 7	1.000
Diastolic dimension (mm)	43 ± 5	44 ± 4	0.204
Systolic dimension (mm)	26 ± 4	27 ± 4	0.182
Ventricular septum (mm)	9.5 ± 1.1	9.3 ± 1.1	0.332
Posterior wall (mm)	9.5 ± 1.4	9.2 ± 1.1	0.168
Left atrium (mm)	33 ± 5	34 ± 5	0.286

diographic abnormalities. Patients with pericardial effusion or anasarca were not included in this study.

Electrocardiograms were obtained within 24 hours of echocardiography, and R- and S-wave amplitudes were measured directly from the standard 12-lead electrocardiograph to the nearest 0.5 mm using calipers and a magnifying glass. The average of 3 QRS complexes (sum of R and S waves) was determined for each lead. Low voltage was defined as a QRS amplitude <5 mm in all limb leads and/or a QRS amplitude <10 mm in all precordial leads. Low voltage was considered present only after diagnosis by 2 cardiologists who had no knowledge of clinical findings. For patients with low voltage, total QRS wave amplitude was defined as the sum of the R- and S-wave amplitudes in 6 limb leads.

Blood samples were taken within <24 hours of the electrocardiogram. Serum albumin was measured by dye-binding bromcresol green procedure and total protein by the Biuret method using a Hitachi 747 analyzer (Hitachi, Tokyo, Japan). Hypoalbuminemia was defined as <38 g/dl. Colloid osmotic pressure was calculated according to the equation by Nitta et al[8] and Staub et al,[9]: [Colloid osmotic pressure = $a(2.8c + 0.18c^2 + 0.012c^3) + b(0.9c + 0.12c^2 + 0.004c^3)$], where "a" is the albumin fraction, "b" is the globulin fraction, and "c" is total protein (grams per liter). Hematocrit was measured by the red blood cell cumulative pulse height detection method using the Sysmex SE 9000 hematology analyser (Sysmex, Kobe, Japan).

An experienced echocardiographer performed M-mode and 2-dimensional echocardiography with a Toshiba SSH 160A phased-array sector scanner

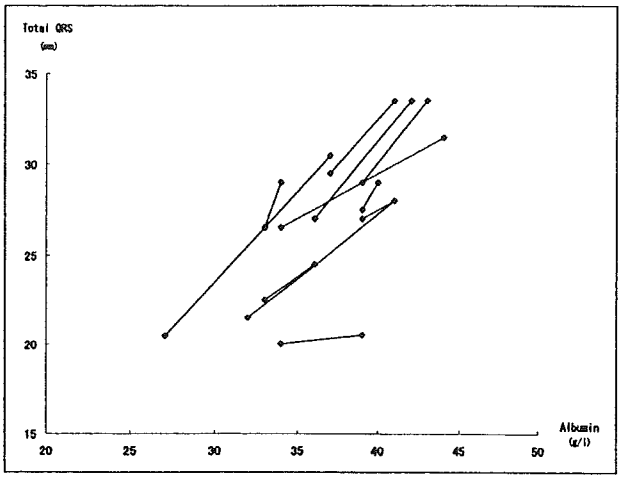

FIGURE 1. Relation of change in total QRS amplitude to change in serum albumin concentration.

(Toshiba, Tokyo, Japan) using a 3.75- or 2.5-MHz transducer. The internal dimension of the left ventricle at end-diastole was measured at the onset of the QRS complex, and the end-systolic dimension was measured at the nadir of septal motion.[10] The thickness of the ventricular septum and posterior wall was measured at the onset of the QRS complex. All classic views were recorded on videotape for subsequent analysis by observers who were unaware of the electrocardiographic data.

Results are reported as mean ± SD. Statistical analysis between the 2 groups was performed by Student's *t* test for continuous variables and Fisher's exact probability test for discrete variables. A paired *t* test was used for paired samples. Regression analysis was used to evaluate the relation between the 2 variables. A p value <0.05 was considered significant.

Among 193 patients, 142 patients were referred to the echocardiographic laboratory to rule out heart disease before operation; 17 patients had connective tissue disease and 34 patients had other noncardiac disorders. Low voltage was detected in 35 patients (18%). Values for albumin and total protein, and colloid osmotic pressure were significantly lower in patients with low voltage compared with those without, but there were no significant differences in the echocardiographic indexes between the 2 groups (Tables 1 and 2). Twenty-seven of 57 patients with hypoalbuminemia had low voltages, whereas 8 of 136 patients without hypoalbuminemia had low voltages. The sensitivity and specificity of low voltages to identify hypoalbuminemia were 47% and 94%, respectively.

In patients with low voltage, there was a fair relation between QRS amplitude and albumin concentration ($r = 0.69$, $p < 0.001$). Follow-up electrocardiography, echocardiography, and serum albumin values were obtained in 11 patients at a mean follow-up of 3.2 ± 2.1 months (0.5 to 6). The serum albumin concentration increased in 9 patients and decreased in 2 patients. Although there were no significant changes in left ventricular diastolic dimension (44 ± 5 vs 44 ± 5 mm), left ventricular systolic dimension (27 ± 6 vs 27 ± 5 mm), septal

thickness (10 ± 1 vs 10 ± 1 mm), and left ventricular posterior wall thickness (10 ± 1 vs 10 ± 1 mm), an increase (decrease) in albumin was accompanied by an increase (decrease) in the total QRS wave amplitude (Figure 1). Moreover, there was a good correlation between the change in total QRS amplitude and the change in albumin concentration ($r = 0.78$, $p = 0.005$).

• • •

The attenuation of QRS wave amplitude is linked to obesity, various lung diseases, and anasarca, whereas augmentation of QRS wave amplitude is associated with a reduction in hematocrit or after hemodialysis.[5–7,11–14] Despite no significant differences in echocardiographic indexes, hematocrit, and body mass index, the serum albumin concentration was significantly lower in patients with low voltages compared with those without. Moreover, low voltage was a highly specific, although not sensitive, electrocardiographic sign of hypoalbuminemia. When the change in albumin concentration and in QRS wave amplitude was assessed, there was a good correlation between these 2 variables. These data indicate that the surface electrocardiographic potentials are attenuated when the resistance of the extracellular space is decreased because of increased extracellular fluid. Thus, serum albumin concentration can affect QRS wave amplitude in patients free of heart and lung diseases.

1. Unverferth DV, Williams TE, Fulkerson PK. Electrocardiographic voltage in pericardial effusion. *Chest* 1979;75:157–160.
2. Spodick DH. The normal and diseased pericardium: current concepts of pericardial physiology, diagnosis and treatment. *J Am Coll Cardiol* 1983;1:240–251.
3. Meyers DG, Bagin RG, Levene JF. Electrocardiographic changes in pericardial effusion. *Chest* 1993;104:1422–1426.
4. Kudo Y, Yamasaki F, Doi T, Doi Y, Sugiura T. Clinical significance of low voltage in asymptomatic patients with pericardial effusion free of heart disease. *Chest* 2003;124:2064–2067.
5. Wagner GS. Marriott's Practical Electrocardiography. 9th Ed. Baltimore: Williams & Wilkins, 1994:176–179.
6. Heaf JG. Albumin-induced changes in the electrocardiographic QRS complex. *Am J Cardiol* 1985;55:1530–1533.
7. Madias JE, Bazaz R, Agarwal H, Win M, Medepalli L. Anasarca-mediated attenuation of the amplitude of electrocardiogram complexes: a description of a heretofore unrecognized phenomenon. *J Am Coll Cardiol* 2001;38:756–764.
8. Nitta S, Ohnuki T, Ohkuda K, Nakada T, Staub NC. The corrected protein equation to estimate plasma colloid osmotic pressure and its development on a nomogram. *Tohoku J Exp Med* 1981;135:43–49.
9. Staub NC. Pathophysiology of pulmonary edema. In: Staub NC, Taylor AE, eds. Edema. New York: Raven Press, 1984:719–746.
10. Henry WL, Gardin JM, Ware JH. Echocardiographic measurements in normal subjects from infancy to old age. *Circulation* 1980;62:1054–1060.
11. Rudy Y, Plonsey R, Liebman J. The effects of variations in conductivity and geometrical parameters on the electrocardiogram, using an eccentric spheres model. *Circ Res* 1979;44:104–111.
12. Rosenthal A, Restieaux NJ, Feig SA. Influence of acute variations in hematocrit on the QRS complex of the Frank electrocardiogram. *Circulation* 1971;44:456–465.
13. Ishikawa K, Nagasawa T, Shimada H. Influence of hemodialysis on electrocardiographic wave forms. *Am Heart J* 1979;97:5–11.
14. Dudley SC, Baumgarten CM, Ornato JP. Reversal of low voltage and infarction pattern of the surface electrocardiogram after renal hemodialysis for pulmonary edema. *J Electrocardiol* 1990;23:341–345.

Japanese Journal of Physiology, 55, 157–163, 2005

Dynamic Characteristics of Carotid Sinus Pressure-Nerve Activity Transduction in Rabbits

Toru KAWADA, Kenta YAMAMOTO, Atsunori KAMIYA, Hideto ARIUMI, Daisaku MICHIKAMI, Toshiaki SHISHIDO, Kenji SUNAGAWA*, and Masaru SUGIMACHI

Department of Cardiovascular Dynamics, Advanced Medical Engineering Center, National Cardiovascular Center Research Institute, Osaka, 565-8565 Japan; and *Department of Cardiovascular Medicine, Graduate School of Medical Sciences, Kyushu University, Fukuoka, 812-8582 Japan

Abstract: The dynamic characteristics of the baroreflex neural arc from pressure input to efferent sympathetic nerve activity (SNA) reveal derivative characteristics in the frequency range of 0.01 to 0.8 Hz (i.e., the baroreflex gain augments with increasing frequency) and high-cut characteristics in the frequency range above 0.8 Hz (i.e., the baroreflex gain decreases with increasing frequency) in rabbits. The derivative characteristics accelerate the arterial pressure regulation via the baroreflex. The high-cut characteristics preserve the baroreflex gain against pulsatile pressure by attenuating the high-frequency components less necessary for arterial pressure regulation. However, to what extent the carotid sinus baroreceptor transduction from pressure input to afferent baroreceptor nerve activity (BNA) contributes to these characteristics remains unanswered. To test the hypothesis that the carotid sinus pressure-BNA transduction partly explains the derivative characteristics but not the high-cut characteristics, we examined the dynamic BNA response to pressure input in the frequency range from 0.01 to 3 Hz by using a white noise analysis in 7 anesthetized rabbits. The transfer function from pressure input to BNA showed slight derivative characteristics in the frequency range from 0.01 to 0.3 Hz with approximately a 1.7-fold increase in dynamic gain, but it showed no high-cut characteristics. In conclusion, the carotid sinus baroreceptor transduction partly explained the derivative characteristics but not the high-cut characteristics of the baroreflex neural arc. The present results suggest the importance of the central processing from BNA to efferent SNA to account for the overall dynamic characteristics of the baroreflex neural arc. [The Japanese Journal of Physiology 55: 157–163, 2005]

Key words: systems analysis, transfer function, baroreflex neural arc.

The carotid sinus baroreflex is among the most important negative feedback systems that stabilize arterial pressure (AP) during daily activity. A knowledge of the dynamic characteristics of a given system is important for an in-depth understanding of the system behavior. In previous studies [1–4], we applied a white noise analysis to the carotid sinus baroreflex in rabbits and assessed the transfer function of the baroreflex neural arc from pressure input to efferent sympathetic nerve activity (SNA). The neural arc transfer function revealed two distinct features. One relates to the derivative characteristics in which the baroreflex gain augments with increasing frequency from 0.01 to 0.8 Hz. The derivative characteristics accelerate the dynamic AP regulation by the carotid sinus baroreflex [1]. The other feature relates to the high-cut characteristics in which the baroreflex gain decreases with increasing frequency above 0.8 Hz [4]. The high-cut characteristics prevent the high-frequency components from saturating the baroreflex central processing and preserve the baroreflex gain against pulsatile pressure. However, whether the carotid sinus

Received on Jun 30, 2005; accepted on Jul 29, 2005; released online on Aug 5, 2005; DOI: 10.2170/jjphysiol.R2122
Correspondence should be addressed to: Toru Kawada, Department of Cardiovascular Dynamics, Advanced Medical Engineering Center, National Cardiovascular Center Research Institute, 5-7-1 Fujishirodai, Suita, Osaka, 565-8565 Japan. Phone:+81-6-6833-5012 (Ext. 2427), Fax: +81-6-6835-5403, E-mail: torukawa@res.ncvc.go.jp

baroreceptor transduction from the pressure input to afferent baroreceptor nerve activity (BNA) or the central processing from the afferent BNA to efferent SNA played a major role in forming derivative and high-cut characteristics remains unanswered.

The dynamic characteristics of the pressure input-nerve activity transduction have been examined by the use of step and sinusoidal inputs [5–7]. Although these classical inputs and resulting outputs are easy to interpret, they have a critical drawback because only limited aspects of the system characteristics can be identified. In other words, the system response to untested input signals cannot be predicted precisely because the untested input signals may have frequency components that the step or sinusoidal input does not have. A white noise input, which is rich in frequency components, is most appropriate for a thorough examination of a given system [8–10]. We have identified the dynamic characteristics from pressure input to aortic depressor nerve activity in rabbits with the white noise analysis [11]. The results of that study suggest that the derivative characteristics of the baroreflex neural arc may be partly attributable to the pressure input-nerve activity transduction, whereas the high-cut characteristics may be primarily attributable to the central processing from BNA to efferent SNA. However, regional differences of the transduction properties have been reported between carotid sinus and aortic baroreceptors [12]. Hence the purpose of the present study was to directly estimate dynamic characteristics of the carotid sinus pressure (CSP)-BNA transduction by using the white noise analysis. The results confirmed the hypothesis that the CSP-BNA transduction partly explained the derivative characteristics, but not the high-cut characteristics.

METHODS

Surgical preparations. The animals were cared for in strict accordance with the Guiding Principles for the Care and Use of Animals in the Field of Physiological Sciences approved by the Physiological Society of Japan. Seven Japanese white rabbits weighing 2.7 to 3.1 kg were anesthetized by intravenous injection (2 ml/kg) of a mixture of urethane (250 mg/ml) and α-chloralose (40 mg/ml), and mechanically ventilated with oxygen-enriched room air. A supplemental dose of these anesthetics was administered continuously (0.5 $ml \cdot kg^{-1} \cdot h^{-1}$) to maintain an appropriate level of anesthesia. AP was monitored by a high-fidelity pressure transducer (Millar Instruments, Houston, TX) inserted via the right femoral artery. Following a midline cervical incision, the right external carotid artery was exposed, ligated at two positions, and sectioned in between to access the tissue between the external and internal carotid arteries. A carotid sinus nerve was identified by using a pair of platinum electrodes and by confirming AP-synchronous activity on a loudspeaker. The nerve was then freed from the platinum electrodes during the following carotid sinus isolation procedure. The right internal carotid artery and other small branches arising from the carotid sinus area were ligated. A catheter (0.6 mm internal diameter, 15 cm long) was introduced from the right common carotid artery, and the carotid sinus blind sac was filled with warmed physiological saline. CSP was measured at the end of the catheter opposite the carotid sinus and was controlled by a servo-controlled piston pump (model ET-126A, Labworks, Costa Mesa, CA). A small amount of leakage from the isolated carotid sinus, if any remained, was replenished from the pump during the experiment. After completing the carotid sinus isolation procedure, we attached a pair of stainless steel wire electrodes to the previously identified carotid sinus nerve (Bioflex wire AS633, Cooner Wire, CA) for the multifiber recording of BNA. The nerve and electrodes were secured with silicone glue (Kwik-Cast, World Precision Instruments, Inc.) for insulation. The preamplified nerve signal was band-pass filtered at 150–1,000 Hz. It was then full-wave rectified and low-pass filtered at 30 Hz to quantify the nerve activity. The left carotid sinus nerve, bilateral aortic depressor nerves, and bilateral vagal nerves were all sectioned. The body temperature of the experimental animal was maintained at approximately 38°C with a heating pad.

In three of the seven animals, the controlled CSP was compared with the actual pressure imposed on the carotid sinus area after the BNA recording experiment had finished. After carefully removing the electrodes and silicone glue, we loosened a ligature to the external carotid artery. A catheter-tip pressure transducer (Millar Instruments, Houston, TX) was then introduced into the carotid sinus from the external carotid artery. A signal from the transducer served as the actual pressure imposed on the isolated carotid sinus area.

Protocols. Random input protocol: We randomly changed CSP to either 80 or 120 mmHg with a switching interval of 50 ms for 15 min in order to estimate the dynamic characteristics of the CSP-BNA transduction.

Stepwise input protocol: We increased CSP from 20 to 180 mmHg every minute with a step size of 20

mmHg in order to estimate the static characteristics of the CSP-BNA transduction.

We recorded CSP, BNA and AP at a sampling rate of 200 Hz by using a 12-bit analog-to-digital converter. The data were stored on the hard disk of a dedicated laboratory computer system for later analysis.

Data analysis. In the random input protocol, we estimated the transfer function, $H(f)$, from CSP input to BNA output according to previous studies [1–4, 8, 10–11, 13]. We normalized the transfer function so that the average transfer gain value below 0.02 Hz became unity and expressed BNA in arbitrary units for dynamic analysis (AU_{dyn}). We also calculated the coherence function, $Coh(f)$, between CSP and BNA [1–4, 8, 10–11, 13]. A unity coherence value indicates perfect linear dependence whereas zero coherence value indicates total independence between CSP and BNA.

In the stepwise input protocol, we calculated the steady-state BNA values by averaging the data during the last 10 s of each CSP level. We then scaled these values so that their minimum and maximum BNA values became 0 and 100 arbitrary units (AU_{stat}), respectively, for static analysis. We performed a regression analysis for the four-parameter logistic function using Eq. 1 [14].

$$y = \frac{P_1}{1+\exp[P_2(x-P_3)]} + P_4 \qquad (1)$$

where P_1 is the response range (i.e., the difference between the maximum and minimum values of y), P_2 is the slope coefficient, P_3 is the midpoint on the input axis, and P_4 is the minimum value of y. The fitting error (err%) for the logistic function was evaluated by using Eq. 2.

$$err\% = \frac{\sum_{k=1}^{N}[u(k)-y(k)]^2}{\sum_{k=1}^{N}[u(k)-\bar{u}]^2} \times 100 \qquad (2)$$

where u(k) and y(k) indicate the measured and predicted BNA values at each CSP level. N indicates the number of data points analyzed, and $\bar{u}$ represents the average value of u(k) when k spans from 1 to N.

RESULTS

The dynamic characteristics of the pressure transduction from CSP to actual pressure imposed on the carotid sinus area are depicted in Fig. 1A. The gain plot (top panel) indicates the ratio of actual pressure to CSP in the frequency domain. The controlled CSP faithfully reflected the actual pressure up to 3 Hz. The ratio was greatly dispersed above 3 Hz. The phase plot (middle panel) indicates that the phase delay was negligible up to 1 Hz. The phase delay at 3 Hz was approximately 0.33 radians. The coherence plot (bottom panel) indicates that the coherence was unity up to 3 Hz and decreased slightly above 3 Hz.

Figure 1B shows a typical time series of CSP and BNA obtained from the random input protocol. CSP was changed according to a binary white noise sequence. BNA varied in response to the CSP input. When CSP was increased, BNA was increased, and vice versa.

Figure 1C illustrates the transfer function from CSP to BNA averaged from all animals. The gain plot (top), phase plot (middle) and coherence plot (bottom) are presented. In each plot the thick line indicates the mean value, and the thin lines indicate the mean ± SEM values. In the gain plot, the gain value at the lowest frequency was normalized to unity. The gain increased with increasing frequency from 0.01 to 0.3 Hz and showed a relatively constant value of approximately 1.7 up to 3 Hz. In the phase plot, the phase value led slightly in the frequency range from 0.01 to 0.2 Hz and close to zero radians from 0.2 to 1 Hz. Although the phase delayed above 1 Hz, the delay is most likely attributable to the phase delay between CSP and actual pressure shown in Fig. 1A. In the coherence plot, the coherence was approximately 0.6 at the lowest frequency and increased to 0.8 in the frequency range of 0.1 to 3 Hz.

Figure 2A depicts the typical time series of CSP and BNA obtained from the stepwise input protocol. The CSP and BNA data were resampled at 2 Hz for these panels. An increase in CSP increased BNA in the CSP range of 40 to 160 mmHg. When the BNA response to stepwise input was obvious, it was greater at the onset of pressure change and then decayed to the steady-state value. The steady-state BNA value was not necessarily greater at 40 mmHg than at 20 mmHg across the animals. The steady-state BNA value was not necessarily greater at 180 mmHg than at 160 mmHg.

Figure 2B illustrates the static input-output relationship between CSP and BNA averaged from all animals. The closed circles and error bars represent mean and mean ± SEM values of BNA at each CSP level, respectively. The solid curve indicates the logistic function constructed from the averaged parameters shown in Table 1.

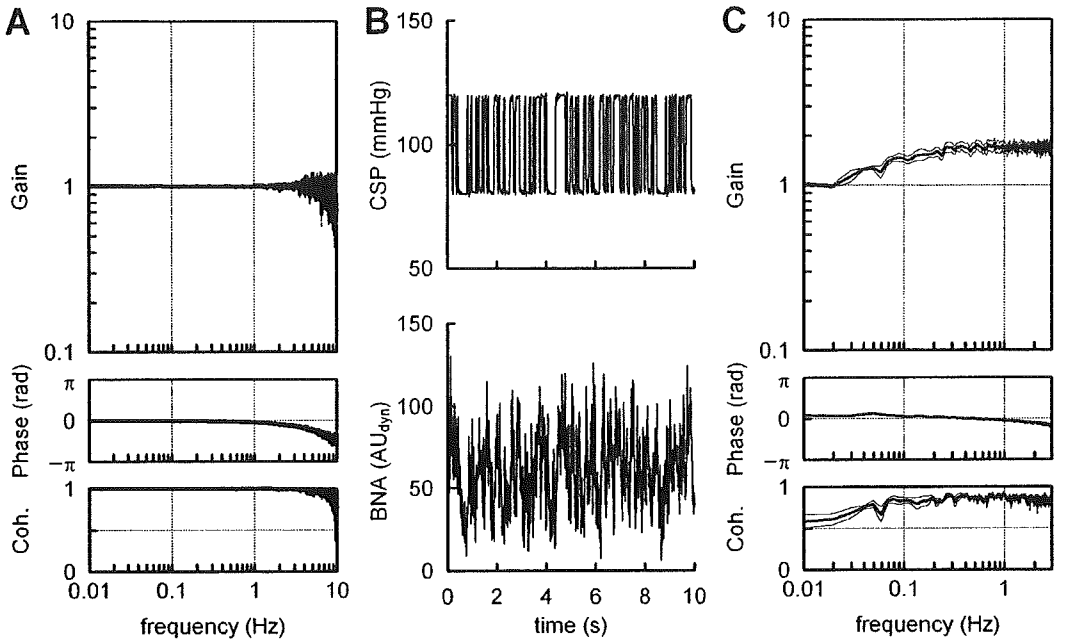

Fig. 1. A: The transfer function from controlled carotid sinus pressure (CSP) to actual pressure imposed on the carotid sinus area. The gain plot represents the ratio of actual pressure to CSP in the frequency domain. The phase plot represents the phase difference between CSP and actual pressure. The coherence (Coh.) shows the extent of linearity between CSP and actual pressure. Based on the transfer function from CSP to actual pressure, we employed the transfer function data up to 3 Hz in the analysis of CSP-nerve activity transduction. The phase difference between CSP and actual pressure in the frequency range between 1 and 3 Hz was taken into account in the interpretation of the CSP-nerve activity transduction. **B: Representative time series of CSP and afferent baroreceptor nerve activity (BNA) during the random input protocol.** CSP was changed according to a binary white noise signal with a switching interval of 50 ms. AU_{dyn}; arbitrary units for dynamic analysis. **C: Transfer function from CSP to BNA averaged from all animals.** The gain plot, phase plot, and coherence are shown. The transfer gain increased with increasing frequency from 0.01 to 0.3 Hz and showed a relatively constant value of approximately 1.7 up to 3 Hz. In all panels, thick and thin lines represent mean and mean ± SEM values.

Table 1 summarizes the parameters of the logistic function fitted to the steady-state CSP-BNA relationship obtained from the stepwise input protocol. The fitting error to the logistic function was less than 1% relative to the total variation in steady-state BNA values.

DISCUSSION

Dynamic characteristics of the carotid sinus baroreceptor transduction. Because of technical difficulty with the in situ preparation, we could not measure actual pressure imposed on the carotid sinus area and record BNA simultaneously. Therefore we measured controlled CSP and actual pressure imposed on the carotid sinus area simultaneously. As shown in Fig. 1A, the controlled CSP faithfully reflected the actual pressure up to 3 Hz. Above this frequency the ratio of actual pressure to CSP became greatly dispersed among animals. Because the compliance of the isolated area would depend on the vascular configuration and inevitably differ among animals, the pressure transduction in the frequencies above 3 Hz may reveal significant inter-individual differences. Actually, the insertion of the catheter-tip micromanometer itself might have affected the compliance of the isolated area to some degree. The phase delay reached approximately 0.33 radians at 3 Hz, which corresponds to 0.018 s of pure dead time. Although this value was not negligible, we employed the transfer function data up to 3 Hz in the analysis of the CSP-BNA relationship because the inter-individual differences in the phase delay were

Table 1. Parameters of the logistic function fitted to the steady-state CSP-BNA relationship.

Response range, P_1, AU_{stat}	98.1 ± 2.4
Slope coefficient, P_2, $mmHg^{-1}$	−0.072 ± 0.010
Midpoint pressure, P_3, mmHg	89.9 ± 3.4
Minimum value, P_4, AU_{stat}	0.05 ± 1.98
err%	0.9 ± 0.5

Data are means±SEM.

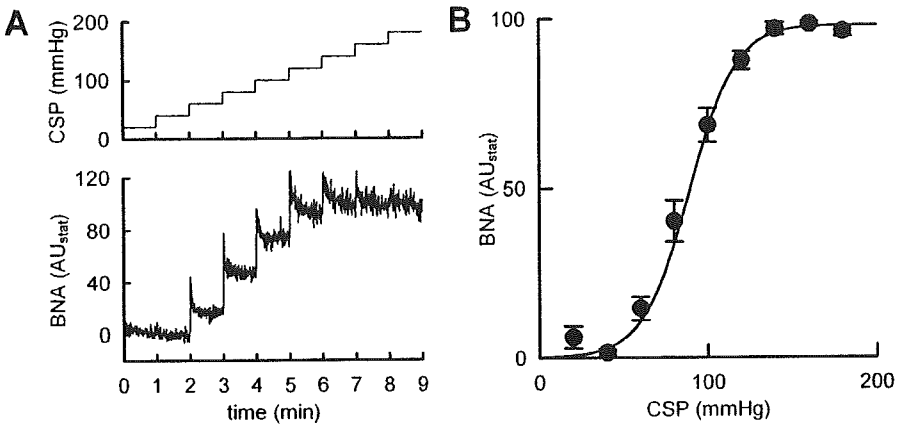

Fig. 2. A: Representative time series of carotid sinus pressure (CSP) and afferent baroreceptor nerve activity (BNA) during the stepwise input protocol. CSP and BNA were resampled at 2 Hz for the panels. CSP was increased from 20 to 180 mmHg every minute with a pressure step of 20 mmHg. **B: The CSP-BNA relationship averaged from all animals.** The CSP-BNA relationship revealed sigmoidal nonlinearity. The closed circles represent mean values, and the error bars indicate mean ± SEM values at each CSP. The solid curve indicates the logistic function derived from averaged parameters shown in Table 1. AU_{stat}: arbitrary units for static analysis.

very small up to 3 Hz. The phase delay between CSP and actual pressure should be taken into account in the interpretation of phase data of the transfer function from CSP to BNA shown in Fig. 1C. The phase delay between CSP and BNA noted in the frequency range above 1 Hz would be chiefly attributable to the phase delay between CSP and the actual pressure imposed on the carotid sinus area.

Derivative characteristics of the baroreflex neural arc contribute to the optimization of the AP regulation by the carotid sinus baroreflex [1]. Although Franz *et al.* [6] reported dynamic characteristics of single baroreceptor fiber activity in the rabbit carotid sinus in the frequency range from 0.078 to 2.5 Hz by using sinusoidal inputs, the derivative characteristics were obscure in that frequency range. As shown in Fig. 1C, dynamic gain from CSP to BNA augmented to approximately 1.7 with increasing frequency from 0.01 to 0.5 Hz, indicating the existence of the derivative characteristics. When the transfer function from CSP input to efferent SNA was identified in our previous study [15], dynamic gain increased to 3.8-fold for cardiac SNA and to 2.3-fold for renal SNA, with increasing frequency from 0.01 to 0.5 Hz (see Fig. 3 in Ref. 15). Thus approximately 40% (for cardiac) and 64% (for renal) of the derivative characteristic may be explained by the dynamic characteristics of the CSP-BNA transduction.

High-cut characteristics of the baroreflex neural arc attenuate high-frequency components in the input pressure and preserve the baroreflex gain against pulsatile pressure [4]. As shown in Fig. 1C, the dynamic gain of the transfer function from CSP to BNA was relatively constant in the frequency range from 0.3 to 3 Hz and showed no high-cut characteristics. Therefore the high-cut characteristics of the baroreflex neural arc are primarily attributable to the central processing from BNA to efferent SNA. In other words, the dynamic characteristics from BNA to efferent SNA should reveal high-cut characteristics with a corner frequency of approximately 0.8 Hz. The mechanism for the putative high-cut characteristics in the central processing remains unclear. The frequency-dependent depression of the signal transduction in the nucleus tractus solitarii (NTS) neurons [16] may be related to the upper frequency limit of central processing. However, the frequency-dependent depression refers to the phenomenon related to the stimulation frequency itself, whereas the high-cut characteristics refer to the attenuation of the system response related to the modulation frequency of the input. Further information is required to reconcile the putative high-cut characteristics and the frequency-dependent depression in the baroreflex central pathway.

The dynamic characteristics of the carotid sinus baroreceptor transduction were generally similar to those of the baroreceptor transduction of the aortic depressor nerve in rabbits [11]. However, a slight difference can be noted as follows. The gain increase from 0.01 to 0.1 Hz was approximately 1.7-fold (4.6 dB/decade) for the carotid sinus baroreceptors (Fig. 1C), whereas it was approximately 2-fold (6.0 dB/decade) for the aortic baroreceptors (see Fig. 5 in Ref. 11). In the rat aortic baroreceptor preparation, Brown *et al.* [5] demonstrated that myelinated fibers showed peaking in the frequency response, whereas unmyelinated fibers did not. The myelinated and unmyelinated fiber composition would affect the dynamic characteristics of multifiber BNA. Brown *et al.* [5] also demonstrated that the peaking of myelinated fiber response reached approximately 4 dB/decade in normotensive rats and approximately 6 dB/decade in spontaneously hyperten-

sive rats. Therefore the difference between the carotid sinus and aortic baroreceptor transductions, though it seems subtle, may reflect the difference in the myelinated and unmyelinated fiber composition and/or the difference in the prevailing pressure between the carotid sinus and aortic baroreceptors.

Static characteristics of the carotid sinus baroreceptor transduction. The static characteristics of the CSP-BNA transduction showed sigmoidal nonlinearity (Fig. 2B). BNA increased with CSP in the pressure range from 40 to 160 mmHg. In the single fiber preparation of the rabbit carotid sinus baroreceptors, the stimulus-response curve is fairly linear in each fiber between threshold pressure and saturation pressure [6]. However, the threshold pressure and the slope of the linear range vary considerably among fibers. Such variations in the static characteristics of single baroreceptor fiber activities are lumped together, possibly forming the sigmoidal relationship between CSP and multifiber BNA. The slope coefficient of the CSP-BNA relationship (Table 1) was smaller than the slope coefficient of the CSP-SNA relationship (0.10–0.12) determined in our previous studies [15, 17, 18]. In other words, the operating range of the system, which is inversely related to the slope coefficient [14], was wider for the CSP-BNA relationship than for the CSP-SNA relationship. The finding is consistent with our speculation, which is based on input-size and operating-point dependence of the baroreflex neural arc transfer function, that the static CSP-BNA relationship alone does not determine the overall nonlinearity of the neural arc characteristics [2, 3].

The midpoint pressure of the CSP-BNA relationship was approximately 90 mmHg, which is lower than the midpoint pressure of the CSP-SNA relationship (100–110 mmHg) determined in our previous studies [15, 17, 18]. The possibility cannot be ruled out, however, that the extensive surgical operation necessary for the BNA recording had altered the mechanical properties of the carotid sinus area differently from the preparation for the carotid sinus isolation alone. Although we had intended to simultaneously record afferent BNA and efferent SNA, the SNA and AP did not respond to the CSP input in the present experimental settings. A large portion of the baroreceptor afferent fibers may have been damaged because of fragility during the preparation. The difficulty results because we could not know, based on the magnitude of BNA, what percent of the nerve fibers were really kept intact. Further efforts are required to directly demonstrate the difference in the static input-output characteristics between the CSP-BNA relationship and the CSP-SNA relationship.

In conclusion, although a slight difference was noted, the dynamic characteristics of the carotid sinus baroreceptor transduction were similar to those of the aortic baroreceptor transduction in rabbits. The CSP-BNA transduction partly explained the derivative characteristics, but not the high-cut characteristics found in the neural arc transfer function from CSP to efferent SNA. The present results suggest the importance of the central processing from BNA to efferent SNA to account for the overall dynamic characteristics of the baroreflex neural arc.

This study was supported by the Health and Labour Sciences Research Grant for Research on Advanced Medical Technology from the Ministry of Health Labour and Welfare of Japan (H14-Nano-002), and by the Program for Promotion of Fundamental Studies in Health Science of the Pharmaceuticals and Medical Devices Agency of Japan.

REFERENCES

1. Ikeda Y, Kawada T, Sugimachi M, Kawaguchi O, Shishido T, Sato T, Miyano H, Matsuura W, Alexander J Jr, and Sunagawa K: Neural arc of baroreflex optimizes dynamic pressure regulation in achieving both stability and quickness. Am J Physiol Heart Circ Physiol 271: H882–H890, 1996
2. Kawada T, Uemura K, Kashihara K, Kamiya A, Sugimachi M, and Sunagawa K: A derivative-sigmoidal model reproduces operating point-dependent baroreflex neural arc transfer characteristics. Am J Physiol Heart Circ Physiol 286: H2272–H2279, 2004
3. Kawada T, Yanagiya Y, Uemura K, Miyamoto T, Zheng C, Li M, Sugimachi M, and Sunagawa K: Input-size dependence of the baroreflex neural arc transfer characteristics. Am J Physiol Heart Circ Physiol 284: H404–H415, 2003
4. Kawada T, Zheng C, Yanagiya Y, Uemura K, Miyamoto T, Inagaki M, Shishido T, Sugimachi M, and Sunagawa K: High-cut characteristics of the baroreflex neural arc preserve baroreflex gain against pulsatile pressure. Am J Physiol Heart Circ Physiol 282: H1149–H1156, 2002
5. Brown AM, Saum W, and Yasui S: Baroreceptor dynamics and their relationship to afferent fiber type and hypertension. Circ Res 42: 694–702, 1978
6. Franz GN, Sher AM, and Ito CS: Small signal characteristics of carotid sinus baroreceptors of rabbits. J Appl Physiol 30: 527–535, 1971
7. Spickler JW and Kezdi P: Dynamic response characteristics of carotid sinus baroreceptors. Am J Physiol 212: 472–476, 1967
8. Marmarelis PZ and Marmarelis VZ: Analysis of Physiological Systems, Plenum, New York, pp 131–221, 1978
9. Kawada T, Fujiki N, and Hosomi H: Systems analysis of the carotid sinus baroreflex system using a sum-of-sinusoidal input. Jpn J Physiol 42: 15–34, 1992
10. Sugimachi M, Imaizumi T, Sunagawa K, Hirooka Y, Todaka K, Takeshita A, and Nakamura M: A new method

to identify dynamic transduction properties of aortic baroreceptors. Am J Physiol Heart Circ Physiol 258: H887–H895, 1990
11. Sato T, Kawada T, Shishido T, Miyano H, Inagaki M, Miyashita H, Sugimachi M, Knuepfer MM, and Sunagawa K: Dynamic transduction properties of in situ baroreceptors of rabbits aortic depressor nerve. Am J Physiol Heart Circ Physiol 274: H358–H365, 1998
12. Pelletier CL, Clement DL, and Shepherd JT: Comparison of afferent activity of canine aortic and sinus nerves. Circ Res 31: 557–568, 1972
13. Bendat J and Piersol A: Random Data 3rd Ed. John Wiley & Sons, New York, pp 189–271, 2000
14. Kent BB, Drane JW, Blumenstein B, and Manning JW: A mathematical model to assess changes in the baroreceptor reflex. Cardiology 57: 295–310, 1972
15. Kawada T, Shishido T, Inagaki M, Tatewaki T, Zheng C, Yanagiya Y, Sugimachi M, and Sunagawa K: Differential dynamic baroreflex regulation of cardiac and renal sympathetic nerve activities. Am J Physiol Heart Circ Physiol 280: H1581–H1590, 2001
16. Liu Z, Chen C, and Bonham AC: Frequency limits on aortic baroreceptor input to nucleus tractus solitarii. Am J Physiol Heart Circ Physiol 278: H577–H585, 2000
17. Kawada T, Uemura K, Kashihara K, Jin Y, Li M, Zheng C, Sugimachi M, and Sunagawa K: Uniformity in dynamic baroreflex regulation of left and right cardiac sympathetic nerve activities. Am J Physiol Regul Integr Comp Physiol 284: R1506–R1512, 2003
18. Yamamoto K, Kawada T, Kamiya A, Takaki H, Miyamoto T, Sugimachi M, and Sunagawa K: Muscle mechanoreflex induces the pressor response by resetting the arterial baroreflex neural arc. Am J Physiol Heart Circ Physiol 286: H1382–H1388, 2004

Acta Physiol Scand 2005, 184, 187–193

Myocardial interstitial choline and glutamate levels during acute myocardial ischaemia and local ouabain administration

T. Kawada,[1] T. Yamazaki,[2] T. Akiyama,[2] T. Shishido,[1] H. Mori[2] and M. Sugimachi[1]

1 *Department of Cardiovascular Dynamics, National Cardiovascular Center Research Institute, Osaka, Japan*

2 *Department of Cardiac Physiology, National Cardiovascular Center Research Institute, Osaka, Japan*

Received 25 November 2004, accepted 16 March 2005
Correspondence: T. Kawada, Department of Cardiovascular Dynamics, National Cardiovascular Center Research Institute, 5-7-1 Fujishirodai, Suita, Osaka 565-8565, Japan.
E-mail: torukawa@res.ncvc.go.jp

Abstract

Aim: Noradrenaline (NA) uptake transporters are known to reverse their action during acute myocardial ischaemia and to contribute to ischaemia-induced myocardial interstitial NA release. By contrast, functional roles of choline and glutamate transporters during acute myocardial ischaemia remain to be investigated. Because both transporters are driven by the normal Na^+ gradient across the plasma membrane in a similar manner to NA transporters, the loss of Na^+ gradient would affect the transporter function, which would in turn alter myocardial interstitial choline and glutamate levels. The aim of the present study was to examine the effects of acute myocardial ischaemia and the inhibition of Na^+,K^+-ATPase on myocardial interstitial glutamate and choline levels.

Methods: In anaesthetized cats, we measured myocardial interstitial glutamate and choline levels while inducing acute myocardial ischaemia or inhibiting Na^+,K^+-ATPase by local administration of ouabain.

Results: The choline level was not changed significantly by ischaemia (from 0.93 ± 0.06 to 0.82 ± 0.13 μM, mean ± SE, $n = 6$) and was decreased slightly by ouabain (from 1.30 ± 0.06 to 1.05 ± 0.07 μM, $P < 0.05$, $n = 6$). The glutamate level was significantly increased from 9.5 ± 1.9 to 34.7 ± 6.1 μM by ischaemia ($P < 0.01$, $n = 6$) and from 8.9 ± 1.0 to 15.9 ± 2.3 μM by ouabain ($P < 0.05$, $n = 6$). Inhibition of glutamate transport by *trans*-L-pyrrolidine-2,4-dicarboxylate (*t*-PDC) suppressed ischaemia- and ouabain-induced glutamate release.

Conclusion: Myocardial interstitial choline level was not increased by acute myocardial ischaemia or by Na^+,K^+-ATPase inhibition. By contrast, myocardial interstitial glutamate level was increased by both interventions. The glutamate transporter contributed to glutamate release via retrograde transport.

Keywords acetylcholine, cardiac microdialysis, cats, coronary artery occlusion, myocardium, noradrenaline.

Acute myocardial ischaemia causes oxygen depletion and loss of ATP in the ischaemic region (Hearse 1979). Blockade of H^+-ATPase leads to noradrenaline (NA) leakage from storage vesicles and axoplasmic NA accumulation (Schömig *et al.* 1988). Intracellular acidosis causes Na^+ influx via Na^+/H^+ exchange. Inhibition of Na^+,K^+-ATPase activity reduces the Na^+ gradient across the plasma membrane. Because NA uptake transporters are driven by the normal Na^+ electrochemical gradient across the plasma membrane,